Measurements and Modeling of Two-Phase Flow in Microchannels With Nearly Constant Heat Flux Boundary Conditions

Lian Zhang, Jae-Mo Koo, Linan Jiang, *Member, IEEE*, Mehdi Asheghi, *Member, IEEE*, Kenneth E. Goodson, *Associate Member, IEEE*, Juan G. Santiago, *Associate Member, IEEE*, and Thomas W. Kenny

***Abstract*—Two-phase forced convective flow in microchannels is promising for the cooling of integrated circuits. There has been limited research on boiling flow in channels with dimensions below 100 μm, in which bubble formation and flow regimes can differ from those in larger channels. This work develops single and multichannel experimental structures using plasma-etched silicon with pyrex glass cover, which allow uniform heating and spatially-resolved thermometry and provide optical access for visualization of boiling regimes. Boiling was observed with less than 5 °C of superheating in rectangular channels with hydraulic diameters between 25 and 60 μm. The channel wall widths are below 350 μm, which minimizes solid conduction and reduces variations in the heat flux boundary condition. Pressure drop and wall temperature distribution data are consistent with predictions accounting for solid conduction and homogeneous two-phase convection. [651]**

***Index Terms*—Heat exchanger, microchannel, two-phase cooling.**

I. Introduction

TWENTY years ago, Tuckerman and Pease [1] predicted that single-phase forced convective cooling in microchannels should be feasible for circuit power densities of more than 1000 W/cm^2, and demonstrated a microchannel heat sink that removes 790 W/cm^2 with 71 °C temperature increase at 600 mL/min flow rate. While subsequent research has focused on modeling and optimization of single-phase liquid microchannel heat exchangers [2], [3], the more complicated physics of boiling flow in microchannels has received little attention. Boiling convection is promising because it requires less pumping power than single-phase liquid convection to achieve a given heat sink thermal resistance. Peng *et al.* investigated flow transition and heat transfer in V-shaped microchannels with hydraulic diameters ranging from 200 to 600 μm [4], [5]. Jiang *et al.* studied phase change in diamond-shaped microchannels with hydraulic diameters less than 100 μm [6]. Peles *et al.* proposed a one-dimensional (1-D) flow model with flat evaporation front dividing the liquid and vapor into two distinct domains based on their experiments with 50 to 200 μm hydraulic diameter channels [7]. Other experimental studies have focused on microchannels with larger hydraulic diameters [8]–[10]. However, more research is needed to better understand the behavior of boiling flow regimes in channels with diameters below 100 μm, in particular the impact of the small dimensions on bubble nucleation and the heat transfer coefficient.

In our previous study [11], nucleate boiling was observed in 55 μm hydraulic diameter microchannels. In order to study the phase change as well as heat transfer in microchannels in more detail, we developed single and multichannel devices which are designed to minimize variations in the heat flux boundary conditions and preheating of the fluid before entry into the channel. This is achieved by reducing the channel wall thickness and modifying flow entrance geometry. The microchannels are integrated on a bridge structure with a single resistor on one side, which serves as both a heater and a series of thermometers. Channel width ranges from 20 to 50 μm, with 50 to 100 μm in depth, giving a range of 25 to 60 μm hydraulic diameters. A glass slide seals the channels and provides optical access to the internal flow conditions.

We developed simulation models for single and two-phase flow heat transfer using finite volume method. Both homogenous flow model and annular flow model were used in two-phase simulation, and the theoretical predictions were compared with experimental results. The homogenous model results are in better agreement with experimental data.

II. Design

Fig. 1 shows the schematic of the test device. The overall dimension is 2 by 6.5 cm. The narrowed bridge design helps to concentrate the heat flux from the resistor to the microchannel region. The outlet is formed in a 3 by 3 mm pad at the end of the channel so that the outlet fluid temperature can be measured with a thermocouple before there is significant heat loss to the surrounding silicon.

Fig. 2 provides more detailed views of the design of the channel region. A 600 -μm wide, 250 -μm deep reservoir is defined at the inlet, with a 2-mm-long entrance region [see Fig. 2(a)]. The entrance region is a part of the microchannel, but not covered by the heater. This design helps to reduce the

Manuscript received June 12, 2000. This work was supported by DARPA through the HERETIC Program under Contract F33615-99-C-1442, and the work of L. Zhang, an A. Earl Cullum and Margaret Bennet Cullum Fellow, was supported under a Stanford Graduate Fellowship. The project made use of the National Nanofabrication Users Network facilities supported by the National Science Foundation under Award ECS-9731294. Subject Editor W. N. Sharpe, Jr.

L. Zhang, J.-M. Koo, L. Jiang, K. E. Goodson, J. G. Santiago, and T. W. Kenny are with the Department of Mechanical Engineering,Terman Engineering Center, Stanford University, Stanford, CA 94305-4021 USA.

M. Asheghi is with the Department of Mechanical Engineering, Carnegie Mellon University, Pittsburgh, PA 15213 USA.

Publisher Item Identifier S 1057-7157(02)00078-1.

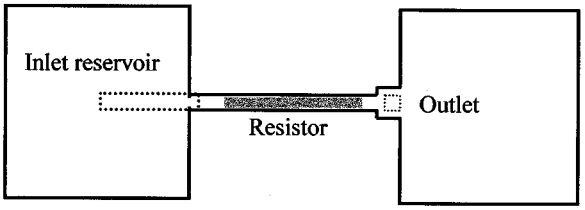

Fig. 1. Schematic of the test device, showing arrangement of inlet and outlet ports and the narrow free standing, instrumented microchannel.

(a)

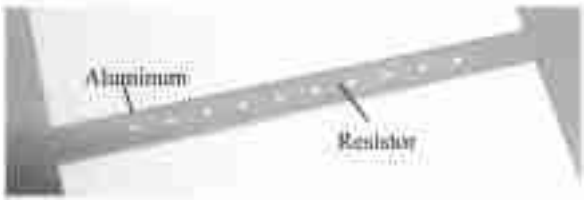

(b)

Fig. 2. Close-up views of microchannels and resistors. (a) Single channel design. (b) Resistors on a multichannel design.

TABLE I
STRUCTURAL PARAMETERS

Structure	Dimension
Inlet reservoir	600 μm wide, 250 μm deep, 1 cm long
Bridge	500 μm (single) / 2 mm (multi) wide, 2 cm long
Single-channel design	40-50 μm wide, 50-100 μm deep, 2 cm long
Multi-channel design	20 μm (width) x 50-70 μm (depth) x 40, 40 μm (width) x 100 μm (depth) x 20, 2 cm long
Resistor (heater)	400 μm wide, 1.6 cm long (single) 1 mm wide, 1.8 cm long (multi) 800 Ω (single) and 360 Ω (multi)

preheating of the fluid. There is a similar exit region at the outlet. A single resistor [see Fig. 2(b)] is formed on the back side of the channel by ion implantation to single crystal silicon. The resistor is divided into nine segments and functions as both a heater and nine thermometers in series. When a current is applied to the resistor, the resistance change of individual segments, corresponding to the change of wall temperature, can be measured by recording the voltage across each segment.

In order to study phase-change in microchannels and boiling uniformity across a group of channels, we have developed both single-channel and multichannel test devices. Design parameters are listed in Table I.

III. FABRICATION

For the current micro-scale heat transfer test devices, we have selected 4-inch, N-type, ⟨100⟩ orientation, 400 -μm thick, and

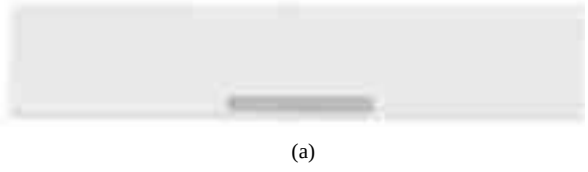

(a)

(b)

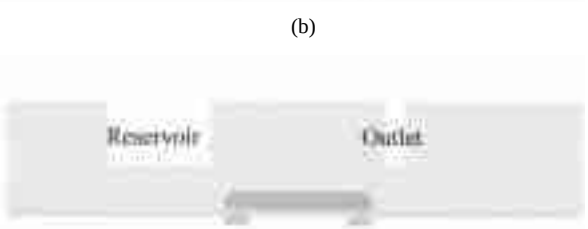

(c)

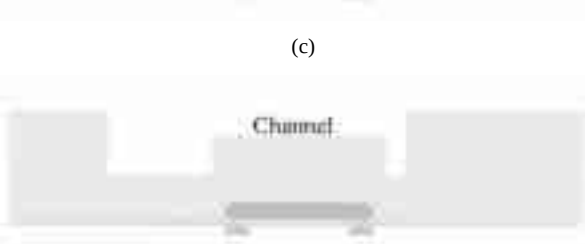

(d)

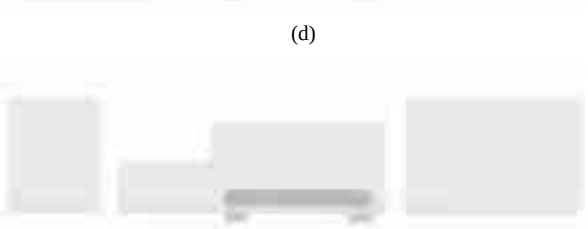

(e)

(f)

Fig. 3. Schematic of fabrication process. (a) Forming the resistor by ion implantation and anealing. (b) Depositing Al pads as contacts (10 in reality). (c) Front side DRIE etching reservoir and outlet. (d) Etching microchannels. (e) Back side etching inlet/outlet through holes. (f) Schematic of fabrication process.

1000 -Ω/cm resistivity silicon wafers as substrates. As shown in Fig. 3, fabrication process begins with ion implantation to form the resistor on the back side. Boron is implanted to the resistor region at 1e16 ions/cm^2 dose and 40 keV energy, with 1.6 μm photoresist as mask. The dopant is then activated and driven in with 15-min wet oxidation at 1100 °C, followed by a six-hour annealing at 1150 °C. The process forms about 2700 Å silicon dioxide to protect the resistor; with approximately 8 μm

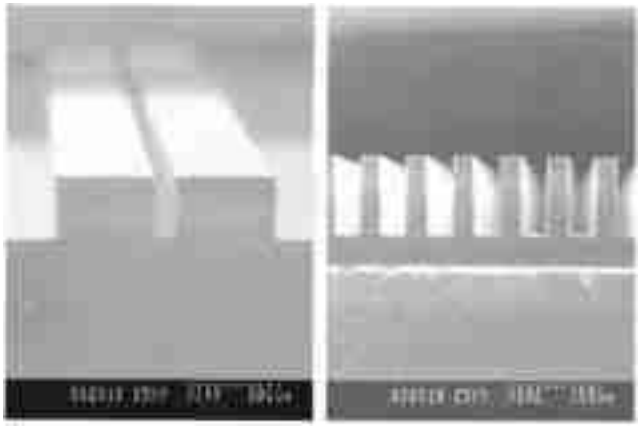

(a) (b)

Fig. 4. SEM images of microchannels. (a) A 40 by 100 μm single-channel design. (b) A 40 parallel 40 by 100 μm multichannel design.

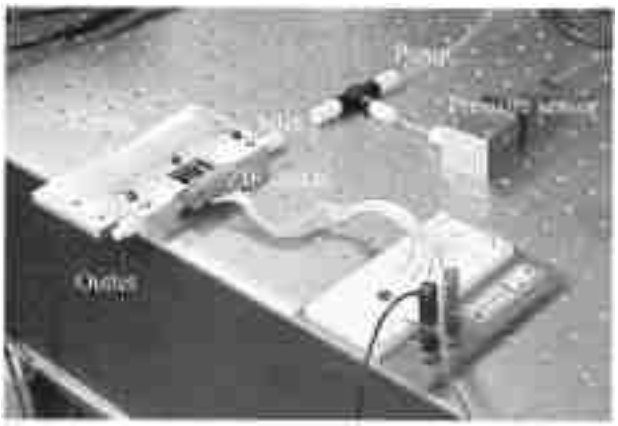

Fig. 5. Photograph of experimental setup, showing microchannel sample mounted in test fixture with electrical connections to the circuit board, and fluidic connections to a syringe pump and a pressure sensor.

junction depth, and 18 $\Omega/\square$ sheet resistance. The deep PN junction with high substrate resistivity can dramatically increase the break-down voltage, which is higher than 100 V in this case.

Next, contact windows are opened through the oxide layer and 99% aluminum with 1% Si is deposited as contacts. Since boron oxide may form during the high-dose annealing process, an argon etch prior to deposition is strongly recommended to form a good contact. After aluminum etch, a freckle etch is performed to remove aluminum freckles from the substrate surface to prevent shorts between contacts. Then the contact is finished by a one-hour forming gas anneal (10% H_2 and 90% N_2) at 400 °C.

The process is then continued with etching the reservoirs and channels from the front side. The 250-μm-deep reservoir and outlet are first DRIE etched into the substrate. Then 7 μm thick photoresist (e.g., SPR220-7 or AZ4620) is used as the channel etching mask, which is thick enough to cover the 250-μm-deep trenches. Channel etching stops at desired depth by a timed etch and inspection, as shown in Fig. 4. Next, the device wafer is bonded to a support wafer with photoresist and etched through. Finally, the device chip is anodically bonded to a prediced Pyrex 7740 piece.

IV. Experimental Setup

As shown in Fig. 5, the device is clamped in a fixture with an internal O-ring to seal the inlet. A pressure transducer is located at the flow entrance of the fixture. Since the internal flow channels in the fixture are much larger than the microchannels, the pressure drop within the fixture can be neglected. The outlet is open to the air and a 100 -μm-diameter thermocouple is fixed right at the outlet of the microchannel to measure exit water temperature. A constant flow rate syringe pump supplies DI water to the system.

The data acquisition system consists of a laptop computer, a 16-bit, 16-channel PCMCIA A/D card, and signal conditioning circuitry. The system is controlled through LabVIEW G programming, capable of continuously scanning the 12 signals at 1000 Hz frequency.

V. Experimental Results

Various devices were tested under constant flow rates. With these experiments, we aim to verify the pressure variation with heating input through the initiation of boiling. We also aim to measure the wall temperature distribution during phase change as supporting data for our flow model.

Measurement results of two devices are presented here. Device 1 is a 40-channel design, each channel is 20 -μm wide and 70-μm deep (31–μm hydraulic diameter). Device 2 is a 50 -μm wide and 70 -μm deep (58 -μm hydraulic diameter) single-channel design. Both results were measured at 0.1 mL/min constant DI wafer flow rate.

A. Thermometer Calibration

Wall temperature change is indicated by the change in resistance of the thermometers. By recording the applied current and voltage difference across each thermometer, we obtain the resistance, hence the temperature. Temperature-resistance curves of each of the nine thermometers on every single device are individually measured and fitted. The resistances are calibrated by placing the silicon chip in a convection oven with a reference thermocouple, and recording the resistance changes in each segment of the resistor as the temperature is raised through the measurement range of 20 to 140 °C. Fig. 6 gives a typical fitting curve, which includes measurement data from six calibration cycles. In all experimental data in the following figures, the main source of error is uncertainty in the thermometer calibration, which is about ± 3 °C.

B. Multichannel Device Measurements

Figs. 7–9 give the pressure and local wall temperature changes against increasing heat power, as well as wall temperature distributions before and after phase change.

In Fig. 7, as we observed before [11], pressure decreases with increasing power during single-phase flow due to the decrease in liquid viscosity with increasing temperature. Just after the onset of boiling, because the density of vapor is much lower than that of water, the local volume flow rate in the channel suddenly increases. The resulting acceleration of the mixture yields a large pressure drop along the channel.

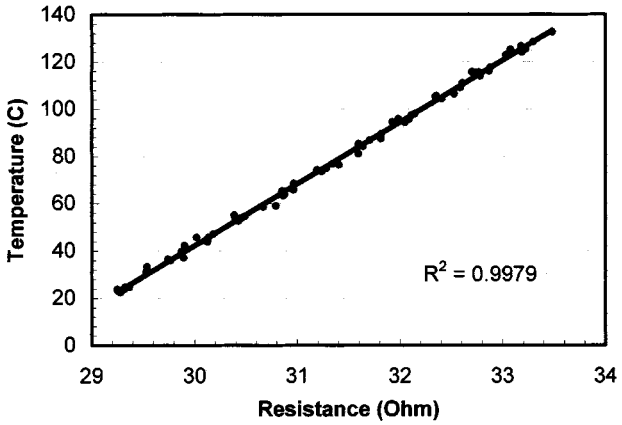

Fig. 6. Thermometer calibration and fitting curve. This figure shows a typical temperature-resistance calibration for one of the resistors in our sample. This figure shows data recorded during six independent calibrations of the same resistor, illustrating repeatability and linearity.

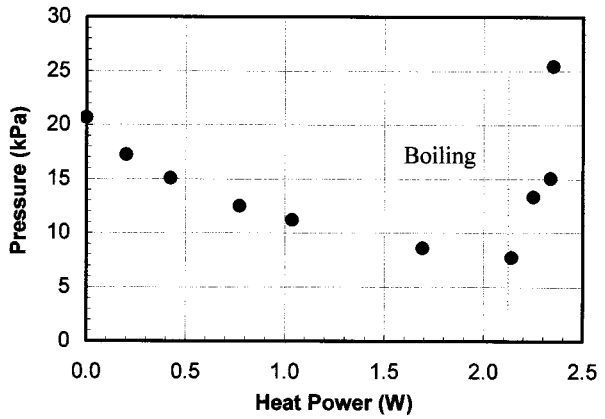

Fig. 7. Pressure change in a 40-channel device, measured as a function of heat power for a fixed DI water flow rate of 0.1 mL/min.

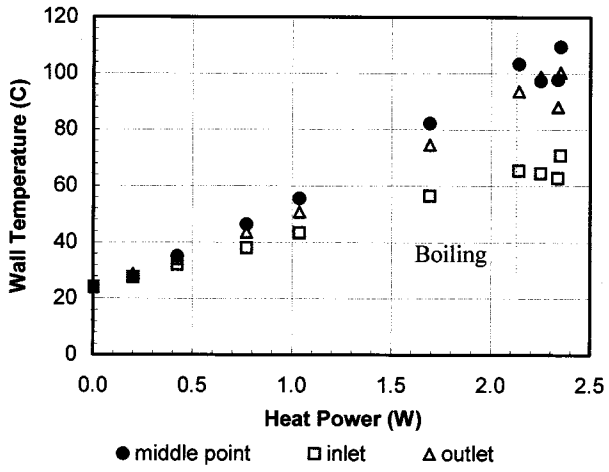

Fig. 8. Local wall temperatures of a 40-channel device, measured as a function of heat power for a fixed DI water flow rate of 0.1 mL/min.

Local wall temperatures are plotted in Fig. 8. Although boiling is quite uniform across the channels, that is, boiling occurs at about the same place in each channel, current and voltage signals at every measurement point begin fluctuating in time after the onset of boiling. The data also indicate a

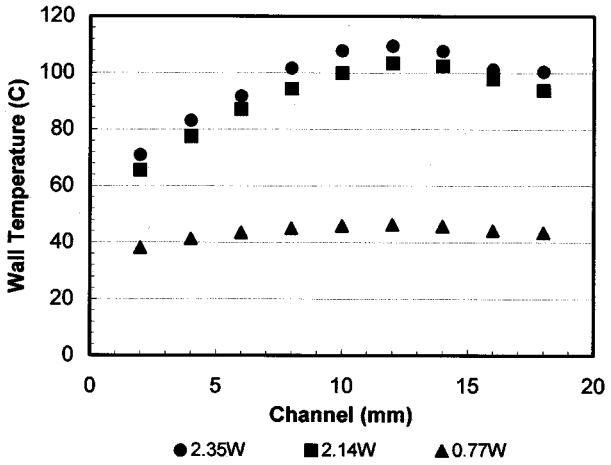

Fig. 9. Wall temperature distributions in a 40-channel device, measured at three heat power levels for a fixed DI water flow rate of 0.1 mL/min. The onset of boiling occurs at 2.14 W heat power.

slight reduction in wall temperature at the initiation of boiling for all of the thermometers. This may be due to the local temperature superheating as a result of nucleation and bubble departure. However, it may also be due to the effect of pressure fluctuations. In work presented elsewhere [12], we show that pressure fluctuations in the microchannel is the main source of small-amplitude resistance changes through a strain effect. Therefore, the onset of these fluctuations in the electrical signals is a very useful indicator of boiling, but the average resistance measurements become more difficult to interpret as temperature measurements. Work is ongoing to understand the relationship between these phenomena in the sensors.

Fig. 9 shows wall temperature distributions at various input power. The parabolic shape results from the conduction losses along the walls into the fluid entrance and exit region.

C. Single-Channel Device Measurements

Figs. 10–12 plot the same measurements performed on a single-channel device. Comparing the results, the pressure curves in Figs. 10 and 7 are similar, except that the onset of boiling in the single channel occurs at a lower heat power (1.32 W) than in multichannels (2.14 W). This is due to the larger heat loss in the multichannel design which will be discussed in the modeling section.

Because of the large change in the pressure distribution along the channel as phase change is occurring, boiling instability could occur if the mass flow rate provided by the pump is coupled with pressure loading. The instability appears as transitions between flow patterns, that is, at some point after boiling begins, the fluid suddenly changes back to liquid phase, then starts boiling again. This cycle usually has a long time period of up to a few minutes. Since the instability affects the flow pattern and heat transfer, the loading capacity should be considered in pump design or selection for microchannel heat exchangers.

Fig. 11 plots the temperature changes of the inlet, outlet and middle point of the channel against increasing heat power. The data indicate no decrease in the wall temperature after the onset of boiling. Once again, it should be emphasized that the uncertainty of the temperature measurements in the two-phase re-

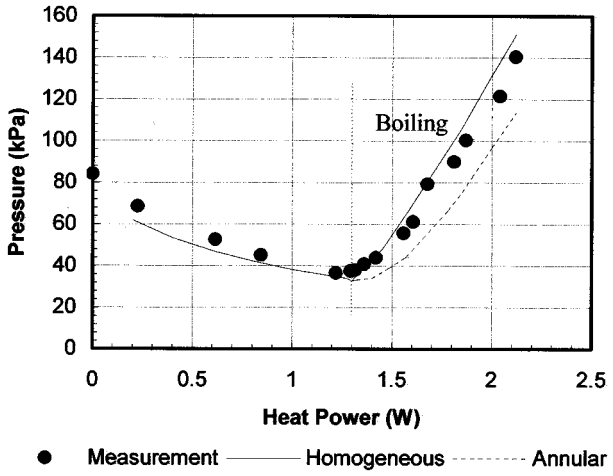

Fig. 10. Measurement and simulations of pressure change in a single-channel device, as a function of heat power for a fixed DI water flow rate of 0.1 mL/min. Both homogeneous and annular flow model simulations are plotted.

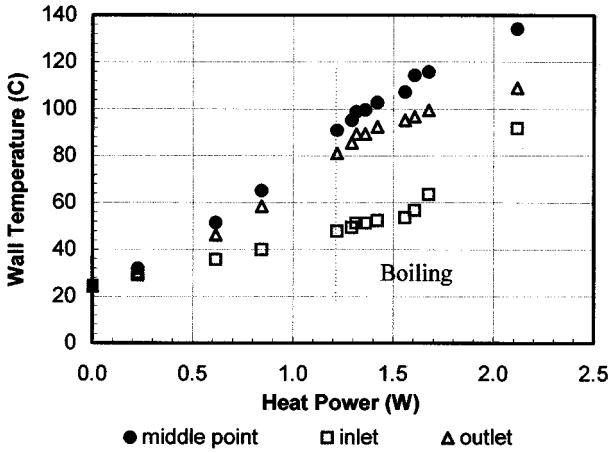

Fig. 11. Local wall temperatures of a single-channel device, measured as a function of heat power for a fixed DI water flow rate of 0.1 mL/min.

gion is increased due to the transient fluctuations in current and voltage signals across the thermometers.

The wall temperature profiles in Fig. 12 are also approximately parabolic, as in the case of the multichannel device. The highest measured wall temperature was 134 °C, which is close to the boiling point of water at the recorded pressure.

Although the phase-change in microchannels is not as stable as in macroscale channels, all our experiments show that nucleation and small bubble growth occur in plasma etched microchannels under 60 μm in hydraulic diameter. No surface condition-induced superheating was measured in these channels. Optical microscopy indicates that the two-phase microchannel flow is mostly annular flow with a very thin layer of liquid. Typical bubbly and plug flow observed in macroscopic channels are absent in these microchannels.

VI. Modeling

The model integrates macroscopic thermal resistances for the test system with microscopic finite volumes for internal microchannel flow. Heat distribution is taken care of in the thermal circuit model, which predicts the fraction of heat carried away

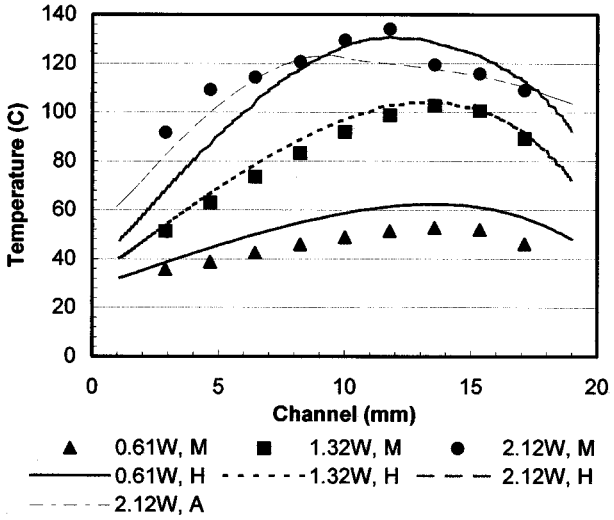

Fig. 12. Measurement and simulation of wall temperature distributions in a single-channel device at three heat power levels for a fixed DI water flow rate of 0.1 mL/min. M refers to measurements, H refers to simulation result from the homogeneous flow model, and A refers to simulation result from the annular flow model.

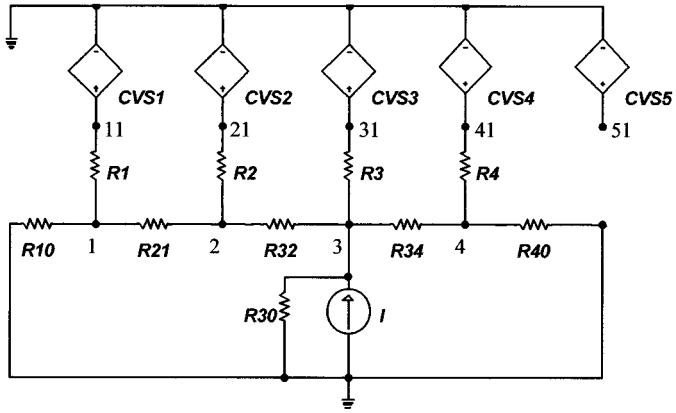

$$CVS1 = I(R1) * Rw/2,$$
$$CVS2 = CVS1 + I(R1) * Rw/2 + I(R2) * Rw/2,$$
$$CVS3 = CVS2 + I(R2) * Rw/2 + I(R3) * Rw/2,$$
$$CVS4 = CVS3 + I(R3) * Rw/2 + I(R4) * Rw/2,$$
$$CVS5 = CVS4 + I(R4) * Rw/2$$

Fig. 13. Schematic of the thermal circuit.

by the microchannel flow. A detailed internal flow model that considers both single and two-phase flow is developed to simulate pressure and temperature distribution with finite volume method. By applying energy balance equations and using classical heat transfer coefficient fittings, the simulation and measurement results are in reasonable agreement.

A. Heat Loss Estimation

A thermal circuit has been developed to estimate the heat loss in the test system. Heat loss here is defined as the fraction of the input power that is carried away by anything other than the fluid.

As shown in Fig. 13, the internal fluid flow (single phase) is modeled as controlled voltage sources (CVS). R_w is the equivalent resistance of convective flow with heat exchange ($1/\dot{m}c_p$, where $\dot{m}$ is the mass flow rate, and c_p is the liquid specific heat).

TABLE II
THERMAL RESISTANCES OF A SINGLE-CHANNEL DEVICE

Resistance	Value (K/W)
R_w ($1/\dot{m}$ c_p, fluid)	143.5
R1 (1/hA, reservoir)	13.8
R2 (1/hA, entrance)	0.5
R3 (1/hA, microchannel)	3.8
R4 (1/hA, exit)	0.5
R21 (l/kA, entrance-reservoir)	80
R32 (l/kA, channel-entrance)	300
R34 (l/kA, channel-exit)	300
R10 (fixture, estimated)	75
R40 (fixture, estimated)	130
R30 (device, estimated)	300

Nodes 1 through 4 are the average temperatures of inlet reservoir, entrance region, microchannel, and the exit region (shown in Figs. 1 and 2). Nodes 11 through 41 are the average temperatures of the fluid in the corresponding sections, and node 51 is the outlet fluid temperature. $R1$ to $R4$ are forced convective resistances ($1/hA$, where h is convective coefficient, and A is convective area); $R10$ and $R40$ represent the sum of device-system contact resistance, system conductive, free convective and radiative resistances; $R30$ is free convective and radiative resistance of the device; $R21$, $R32$, and $R34$ are conductive resistances in silicon (l/kA, where l is the length, k is thermal conductivity of silicon, and A is cross-sectional area).

Ideally, all heat power, which is modeled as the current source I, should go through $R3$ (forced convection in the microchannel) and cause fluid temperature rise. However, there exists heat loss from the device as well as the system in reality, which is reflected by the current in other resistors in the circuit. By simulating the current in all resistors, we can predict the heat distribution in the system.

The thermal circuit analysis suggests that the system heat loss due to conduction in silicon can be limited by adjusting the ratio of $R3$ to other resistors, that is, changing the geometry of the test chip. The model has been used to design the dimensions of the reservoir and channel wall thickness so as to maximize the thermal conduction resistance in these regions. As an example, Table II lists the resistance values of Device 2, a 50 -μm wide and 70 -μm deep single-channel design, at 0.1 mL/min flow rate.

The thermal resistance for conduction through the silicon between the resistor and the fluid-wall interface is approximately 0.23 K/W (single-channel) or 0.06 K/W (multichannel), while the convection resistance into the fluid is never smaller than 3.8 K/W. As a result, the thermometers provide an accurate measure of the wall temperature.

The model also suggests that increasing flow rate is an effective method to reduce heat loss. For example, at 0.5 mL/min flow rate, the system heat loss in Device 1 is as low as 5%, with 5% preheating. However, large flow rates may be detrimental because the local temporal pressure increase during phase change is severe in microchannels in this dimension. Even silicon-glass bonds that survive 500 kPa static pressure could be broken by the boiling, which has been observed in our experiments. Therefore, we chose 0.1 mL/min flow rate in above experiments. Larger flow rates will be tested in future studies.

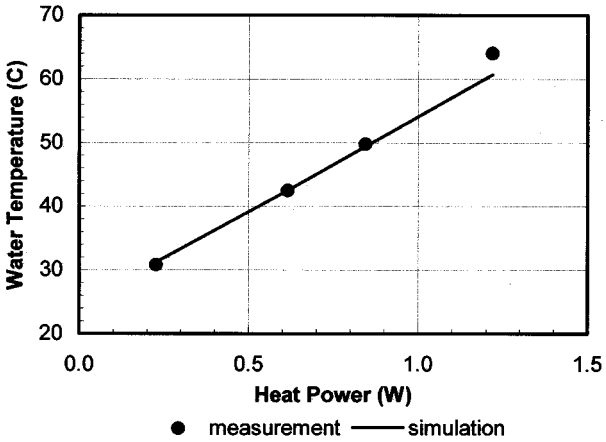

Fig. 14. Outlet water temperature measurement and simulation.

The measured and estimated exit water temperature during single-phase heat transfer experiments on Device 2, are plotted together in Fig. 14. The measurements and simulations are in good agreement, indicating that the model accounts well for the various heat transfer paths in the device. We use this model to estimate the fraction of the system heat loss to the fixture and environment as well as the fraction of the heat carried away by the fluid.

At 0.1 mL/min flow rate, the estimated system heat loss for Device 1 (40-channel design) is 39%, with 20% lost to preheating of inlet water. The system heat loss for Device 2 (single-channel design) is 26%, with 12% lost to preheating.

With the thermal circuit model, we have an accurate description of the heat transfer in the system during single-phase fluid behavior. Therefore, we can now focus on the heat transfer inside the microchannel in the two-phase case.

B. Phase Change Simulation

A 1-D microchannel flow and heat transfer simulation is developed for comparison with the experimental results [13]. The simulation numerically solves energy equations for heat conduction in the silicon wall and convection by the fluid, with boundary conditions dictated by the heat loss to the environment. The simulation uses the finite volume method and considers the temperature and pressure dependence of the liquid and vapor properties based on correlations to tabulated data.

The simulation is 1-D in the direction along the channel and uses average local temperatures for the solid wall and the fluid, T_w and T_f, respectively. The energy equations are

$$\frac{d}{dz}\left(k_w A_w \frac{dT_w}{dz}\right) - \eta h_{\text{conv}} p(T_w - T_f) - \frac{w(T_w - T_\infty)}{R_{env}} + q'' w = 0 \quad (1)$$

$$\dot{m}\frac{di_f}{dz} - \eta h_{\text{conv}} p(T_w - T_f) = 0 \quad (2)$$

where z is the coordinate along the channel, A_w is the channel wall cross-sectional area, p is the perimeter of the channel cross section, and w is the pitch of one channel. The fin effectiveness, η, accounts for the temperature variation normal to the heat sink within the local channel walls. k_w is the thermal conductivity of

silicon, $\dot{m}$ is the mass flow rate, and $h_{\rm conv}$ is the convection coefficient for heat transfer between the channel wall and the fluid. The fluid enthalpy per unit mass, i_f, for two-phase flow is expressed in terms of local fluid quality x, which is the mass fraction of the vapor phase, using

$$i_f = (1-x)i_l + xi_v \tag{3}$$

where subscripts l and v refer to liquid and vapor phase in two-phase flow, respectively. Equation (1) accounts for heat conduction along silicon wall in the first term, convection heat transfer rate in the second term, and the natural convection heat loss to the environment using the resistance $R_{\rm env}$ in the third term. Radiation heat loss is neglected due to its very small magnitude. The fluid flow equation (2) relates the change of the average enthalpy density of the fluid against the heat transfer rate into the fluid from the channel walls.

Two flow models are proposed for the two-phase regime. A homogeneous flow model assumes that the liquid and vapor have the same velocity at every position z. The other approach is annular two-phase flow model, which assumes that a thin, slow-moving liquid film surrounds a rapidly moving core of vapor. The data of Stanley *et al.* [14] for heat flux and friction coefficient for two-phase flow along channels of comparable dimensions lend more support to the homogeneous flow model. The pressure distribution is governed by

$$-\left(\frac{dP}{dz}\right) = \frac{fm''^2}{2\rho D} + \frac{d}{dz}\left(\frac{m''^2}{\rho}\right) \tag{4}$$

for the homogeneous model and by

$$-\left(\frac{dP}{dz}\right) = \frac{2\tau_i}{D/2-\delta} + \frac{m''^2}{\alpha}\frac{d}{dz}\left(\frac{x^2}{\alpha\rho_v}\right) \tag{5}$$

for the annular model, respectively. ρ is the density of the liquid-vapor mixture, ρ_v is the density of vapor phase, f is the globally averaged friction factor, and D is the channel hydraulic diameter. The mass flux m'' is related to the mass flow rate $\dot{m}$ by $m'' = \dot{m}/A_c$, where A_c is the cross-sectional area of the flow passage. δ is the liquid film thickness, τ_i is the shear stress at liquid-vapor interface in annular flow model, and α is void fraction, which is the ratio of the vapor flow cross-sectional area to the total flow cross-sectional area. The friction factor f and the convection coefficient are taken from experimental correlations and are discussed in detail in [13].

The experimental data are compared with the simulation results in Figs. 10 and 12. Fig. 10 shows reasonably good agreement between predictions and measurement data for the pressure drop as a function of applied heat power, particularly for the homogeneous model. The decreasing of the pressure drop with increasing power for powers below 1.32 W results from the decreasing viscosity of the purely liquid phase. The calculations underpredict the pressure drop in this regime due to fluid preheating in the inlet reservoir. The pressure increase with increasing power in the two-phase regime results from the acceleration of the evaporating liquid into the vapor phase. The annular flow model yields less pressure drop than the homogeneous model since it does not include the mixing effect on pressure drop.

Fig. 12 compares predictions and experimental data for the wall temperature distribution along the channel. Relatively poor agreement exists in the middle of the channel for 0.61 W power and the entry region for 2.12 W. The deviation for 0.61 W almost certainly results from an error in the value of the environmental thermal resistance, $R_{\rm env}$ in (1). The deviation for 2.12 W is probably due to the effects of liquid preheating. The simulations are reasonably effective at predicting the temperature magnitude and the onset of boiling. Although they do not provide sufficient detail to choose between the annular and homogeneous models, the pressure drop data lend support to the homogeneous model. Since the pressure field evaluated by the annular flow model is lower than that of homogeneous model, its corresponding saturated-temperature field is also lower than that of homogeneous model. The qualitative agreement provides support for the convection coefficient correlation, which has not previously been applied to channels with hydraulic diameters below 500 μm.

VII. Conclusion

We have developed silicon test devices with nearly-constant heat flux boundary conditions to study forced boiling convection in microchannels. Rectangular channels with hydraulic diameters between 25 and 60 μm and aspect ratios between 1 and 3.5 were fabricated and tested, and we recorded the pressure and wall temperature distribution during phase change. A thermal circuit model and a detailed two-phase microchannel flow model yielded predictions in reasonable agreement with the measured pressure drop and wall temperature distribution. Both models should prove very useful for microchannel design. The experiments show that boiling occurs in plasma-etched microchannels with these dimensions without excessive superheating.

Acknowledgment

The authors wish to thank E. Towe of DARPA/ETO and S. Benning of AFRL/IFSC for their technical input and project management; S. Banerjee for designing and machining the fixture; P. Zhou for helping with experimental setup; R. King, A. Partridge, E. Chow, N. Latta, J. Shott, J. McVittie, and P. Griffin at Stanford University for their great help with the device fabrication.

References

[1] D. B. Tuckerman and R. F. W. Pease, "High-performance heat sinking for VLSI," *IEEE Electron Device Lett.*, vol. EDL-2, pp. 126–129, May 1981.

[2] V. K. Samalam, "Convective heat transfer in microchannels," *J. Electron. Mater.*, vol. 18, no. 5, pp. 611–618, Sept. 1989.

[3] R. W. Knight, D. J. Hall, J. S. Goodling, and R. C. Jaeger, "Heat sink optimization with application to microchannels," *IEEE Trans. Compon., Hybr., Manufact. Technol.*, vol. 15, pp. 832–842, Oct. 1992.

[4] X. F. Peng, H. Y. Hu, and B. X. Wang, "Boiling nucleation during liquid flow in microchannels," *Int. J. Heat Mass Transfer*, vol. 41, no. 1, pp. 101–106, Jan. 1998.

[5] ——, "Flow boiling through V-shaped microchannels," *Experimental Heat Transfer*, vol. 11, pp. 87–100, Mar. 1998.

[6] L. Jiang and M. Wong, "Phase change in microchannel heat sinks with integrated temperature sensors," *J. Microelectromech. Syst.*, vol. 8, pp. 358–365, Dec. 1999.

[7] Y. P. Peles, L. P. Yarin, and G. Hetsroni, "Steady and unsteady flow in a heated capillary," *Int. J. Multiphase Flow*, vol. 27, no. 4, pp. 577–598, Apr. 2001.
[8] D. B. R. Kenning and Y. Yan, "Saturated flow boiling of water in a narrow channel: Experimental investigation of local phenomena," *IChemE Trans. A, Chem. Eng. Res. Design 79 (A4)*, pp. 425–436, May 2001.
[9] R. Hopkins, A. Faghri, and D. Khrustalev, "Critical heat fluxes in flat miniature heat sinks with micro capillary grooves," *J. Heat Transfer*, vol. 121, no. 1, pp. 217–220, Feb. 1999.
[10] M. B. Bowers and I. Mudawar, "High flux boiling in low flow rate, low pressure drop mini-channel and micro-channel heat sinks," *Int. J. Heat Mass Transfer*, vol. 37, no. 2, pp. 321–332, Jan. 1994.
[11] L. Zhang, S. S. Banerjee, J. Koo, D. J. Laser, M. Asheghi, K. E. Goodson, J. G. Santiago, and T. W. Kenny, "A micro heat exchanger with integrated heaters and thermometers," in *Proc. Solid State Sensor and Actuator Workshop*, June 2000, pp. 275–280.
[12] L. Zhang, J. Koo, L. Jiang, K. E. Goodson, J. G. Santiago, and T. W. Kenny, "Study of boiling regimes and transient signal measurements in microchannels," in *Proc. Transducers'01*, vol. 2, June 2001, pp. 1514–1517.
[13] J. Koo, L. Jiang, L. Zhang, P. Zhou, S. S. Banerjee, T. W. Kenny, J. G. Santiago, and K. E. Goodson, "Modeling of two-phase microchannel heat sinks for VLSI chips," in *Proc. Int. MEMS Workshop*, Jan. 2001, pp. 422–426.
[14] R. S. Stanley, R. F. Barron, and T. A. Ameel, "Two-phase flow in microchannels," in *Proc. ASME IMECE*, vol. DSC-62, Nov. 1997, pp. 143–152.

Lian Zhang received the B.S. degree in engineering from Beijing Institute of Technology in 1994, and the M.S. degree in mechanical engineering from Tsinghua University, China, in 1997. She has been working toward the Ph.D. degree in mechanical engineering at Stanford University, Stanford, CA, since 1997 under a Stanford Graduate Fellowship. She worked on piezoresistive microflow sensors as her Master's thesis.

Her current research interests include MEMS sensor design, thermal management for high-power electronics, and individual chip cooling technology such as microchannel and microjet impingement cooling.

Jae-Mo Koo received the B.S. and M.S. degrees in mechanical engineering from Hongik University, Seoul, Korea, in 1994 and 1996, respectively. He received the M.S. degree from the University of Wisconsin, Madison, in mechanical engineering in 1999.

From 1997 to 1998, he worked for Korea Institute of Science and Technology, Seoul, Korea. Currently, he is working toward the doctoral degree at Mechanical Engineering Department, Stanford University, Stanford, CA. His research interests are focused on the microscale heat transfer, microfluidics, MEMS, advanced electronic cooling technology, and electronic/MEMS packaging.

Linan Jiang (S'99–M'00) received the B.S. and M. S. degrees in aerodynamics from Nanjing University of Aeronautics and Astronautics, China, in 1987 and 1990, respectively, and the Ph.D. degree from The Hong Kong University of Science and Technology, in 1999.

She is currently a Research Associate at Stanford University with Department of Mechanical Engineering. Her current research interests include microscale heat transfer and fluid mechanics, novel microdevices and integrated microsensors, advanced cooling technology, electronic/MEMS packaging technology, and advanced micromachining technology.

Mehdi Asheghi (M'00) received the mechanical engineering degree from Sharif University of Technology and the Ph.D. degree from Stanford University, Stanford, CA, in 1999.

In 2000, he joined Carnegie Mellon University, Pittsburgh, PA, where he is now an Assistant Professor. His research interests include the thermal design of transistors, sensors, and actuators for integrated circuits, magnetic writing devices and microelectromechanical systems (MEMS) as well as the fundamental study of heat transport in very small length and/or time scales. He has made contributions to the understanding of thermal transport in thin silicon layers by measuring the thermal conductivity of nearly pure and doped single crystalline silicon layers in the order of one micron thickness, and by refining a theory that accounts for the reduction in thermal conductivity of silicon layers due to size effect and additional impurities.

Kenneth E. Goodson (M'95–A'96) received the B.S., M.S., and Ph.D. degrees in mechanical engineering from the Massachusetts Institute of Technology (MIT), Cambridge, in 1989, 1991, and 1993, respectively.

Currently, he is an Associate Professor of Mechanical Engineering at Stanford University, Stanford, CA. Previously, he worked with the Materials Research Group at Daimler–Benz AG on the thermal design of power circuits. In 1994, he joined Stanford University, where his research group studies thermal transport phenomena in electronic micro- and nanostructures. His research has yielded 80 journal and conference papers and four book chapters.

Dr. Goodson has received the ONR Young Investigator Award and the NSF CAREER Award in 1996, Best Paper Awards at SEMI-THERM in 2001, and the Multilevel Interconnect Symposium in 1998. In 1996, he was a JSPS Visiting Professor at the Tokyo Institute of Technology. In 1999, he received the Outstanding Reviewer Award from the *ASME Journal of Heat Transfer*.

Juan G. Santiago (M'99–A'99) received the Ph.D. degree in mechanical engineering from the University of Illinois at Urbana-Champaign (UIUC).

From 1995 to 1997, he was a Senior Member of the Technical Staff at the Aerospace Corporation and from 1997 to 1998, he was a Research Scientist at UIUC's Beckman Institute. Since 1998, he has been an Assistant Professor of Mechanical Engineering at Stanford University, Stanford, CA, where he specializes in microscale fluid mechanics, microscale optical flow diagnostics, and microfluidic system design. His research includes the investigation of transport phenomena and optimization of systems involving microscale fluid pumping, electrophoretic injections and separations, sample concentration methods, and rapid micromixing processes. The applications of this research include microfabricated bioanalytical systems for drug discovery and cooling systems for microelectronics.

Thomas W. Kenny received the B.S. degree in physics from the University of Minnesota, Minneapolis, in 1983 and the M.S. and Ph.D. degrees in physics from the University of California, Berkeley, in 1987 and 1989, respectively.

He has worked at the Jet Propulsion Laboratory, where his research focused on the development of electron-tunneling-based microsensors and instruments. Since 1994, he has been on the Faculty of the Mechanical Engineering Department, Stanford University, Stanford, CA. He currently oversees graduate students in the Stanford Microstructures and Sensors Laboratory, whose research activities cover a variety of areas such as advanced tunneling sensors, piezoresistive sensors, cantilever arrays, fracture in silicon, and the mechanical properties of biomolecules, cells, insects, and small animals. This group is collaborating with researchers from the IBM Almaden and Zurich Research Centers on nuclear magnetic resonance microscopy and AFM thermomechanical data storage, and with the Bosch RTC on inertial sensors and packaging, and with Intel on fluidic cooling technologies for integrated circuits.